Exotic Superconducting Phases of Ultracold Atom Mixtures on Triangular Lattices

L. Mathey[1], S. -W. Tsai[2], and A. H. Castro Neto[3]
[1] *Physics Department, Harvard University, Cambridge, MA 02138*
[2] *Department of Physics and Astronomy, University of California, Riverside, CA 92521*
[3] *Department of Physics, Boston University, 590 Commonwealth Ave., Boston, MA 02215*
(Dated: February 6, 2008)

We study the phase diagram of two-dimensional Bose-Fermi mixtures of ultracold atoms on a triangular optical lattice, in the limit when the velocity of bosonic condensate fluctuations is much larger than the Fermi velocity. We contrast this work with our previous results for a square lattice system in Phys. Rev. Lett. **97**, 030601 (2006). Using functional renormalization group techniques we show that the phase diagrams for a triangular lattice contain exotic superconducting phases. For spin-1/2 fermions on an isotropic lattice we find a competition of s-, p-, extended d-, and f-wave symmetry, as well as antiferromagnetic order. For an anisotropic lattice, we further find an extended p-wave phase. A Bose-Fermi mixture with spinless fermions on an isotropic lattice shows a competition between p- and f-wave symmetry. These phases can be traced back to the geometric shapes of the Fermi surfaces in various regimes, as well as the intrinsic frustration of a triangular lattice.

PACS numbers: 03.75.Hh,03.75.Mn,05.10.Cc

I. INTRODUCTION

During the last decade there has been remarkable progress in controlling and manipulating ensembles of ultracold atoms[1,2,3]. Using optical lattices and different types of atoms, a variety of non-trivial many-body states can be 'engineered' that are very accurate realizations of Hubbard models. The experimental observation of the Mott-Hubbard superfluid-insulator transition[4], of fermionic superfluids[5], of the Tonks-Girardeau gas[6] and other Luttinger liquids[7], the measurement of noise correlations[8], instabilities[9] as well as localization effects[10] in Bose-Fermi mixtures (BFM), have created a great deal of excitement in the physics community. These findings have prompted a large amount of theoretical work that study charge density wave (CDW) order[11], many-body states of composite particles[13], polaronic effects[14], and tuning of Feshbach resonances on lattices[15].

It is known that the geometric shape of the lattice is a crucial factor in determining the properties of interacting many-body systems. For instance, localized spins interacting antiferromagnetically on a triangular lattice suffer from the phenomenon of *frustration*, when antiferromagnetic order cannot be achieved because of the particular lattice structure. For itinerant fermionic systems, the lattice structure, together with the dispersion relation and the filling fraction, determine the shape of the Fermi surface (FS). The FS, by its turn, is a crucial factor in determining what type of orders the system can develop. Indeed, for the triangular lattice we consider in this paper, which shows a rich and subtle competition between superconducting phases with different symmetries, we find that small changes in the shape of the FS determine which pairing symmetry is dominant. This is a reflection of the "lattice frustration" on the superconducting phases. In solids, this intriguing lattice geometry is realized in materials such as cobaltates[17], transition metal dichalcogenides[18] and κ-$(ET)_2X$ layered organic crystals[19] (if each lattice site is represented by one ET dimer[20]), and has been the subject of several theoretical studies[21,22].

The versatile technology of optical lattices allows to create and tune a vast number of lattice geometries for ultracold atoms, and is therefore a promising experimental environment to study the rich many-body physics that can be engineered within these systems. We study mixtures of ultracold fermionic atoms (either with two hyperfine states that are labeled by pseudo-spin $\uparrow$ and $\downarrow$, or single component, spinless, fermions), and single component bosons on a triangular lattice. Such a system can be realized as a ^{40}K-^{87}Rb mixture in an optical lattice created by Nd:YAG lasers, with tunable interactions. The geometry of the lattice under consideration is shown in Fig. 2 a).

This paper is organized as follows: In section II we derive the effective Hamiltonian for the fermionic degrees of freedom, in the limit of fast condensate modes. In section III we describe the functional renormalization group approach and its implementation. In section IV and V we describe BFMs with spin 1/2 on an isotropic and an anisotropic lattice, respectively, and in section VI we consider spinless fermions. In the last section VII we comment on the detection of the phases found in this paper, and conclude.

II. EFFECTIVE HAMILTONIAN

BFMs in optical lattices are well described by a Hubbard model of the form,

$$H = -\sum_{\langle ij\rangle_{n=1,2},s} t_{f,n} f^\dagger_{i,s} f_{j,s} - \sum_{\langle ij\rangle_{n=1,2}} t_{b,n} b^\dagger_i b_j$$

$$-\sum_i(\mu_f n_{f,i}+\mu_b n_{b,i})+\sum_i\Big[U_{ff}n_{f,i,\uparrow}n_{f,i,\downarrow} +\frac{U_{bb}}{2}n_{b,i}n_{b,i}+U_{bf}n_{b,i}n_{f,i}\Big], \quad (1)$$

where $f^\dagger_{i,s}$ ($f_{i,s}$) creates (annihilates) a fermion at site i with pseudo-spin s ($s=\uparrow,\downarrow$), $b^\dagger_i$ (b_i) creates (annihilates) a boson at site i, $n_{f,i}=\sum_s f^\dagger_{i,s}f_{i,s}$ ($n_{b,i}=b^\dagger_i b_i$) is the fermion (boson) number operator. With this Hamiltonian we describe a BFM with spin 1/2 fermions, whereas a Hamiltonian of a BFM with spinless fermions can be obtained from this Hamiltonian by suppressing the spin indices. Here we allowed for two different values for the hopping amplitudes, for the two types of lattice bonds $\langle ij\rangle_1$ and $\langle ij\rangle_2$. For a triangular lattice, $t_{f,a}$ and $t_{b,a}$ with $a=1,2$ are the fermionic and bosonic tunneling amplitudes between neighboring sites, where the index $a=1$ ($a=2$) refers to the continuous (dashed) bonds, as shown in Fig. 2 a). For the description of the isotropic case we equate $t_{b/f,1}$ and $t_{b/f,2}$, and define $t_f\equiv t_{f,1}=t_{f,2}$ and $t_b\equiv t_{b,1}=t_{b,2}$. μ_f (μ_b) is the chemical potential for fermions (bosons), U_{bb}, U_{ff}, and U_{bf} are the on-site boson-boson, fermion-fermion and boson-fermion repulsion energy, respectively.

We consider the limit of weakly interacting bosons, in which the bosons form a BEC, for which we use the standard Bogoliubov description. Specifically, we assume that a macroscopic number N_0 of bosons is condensed in the $k=0$ mode, which we take into account by replacing the operator b_0 by $\sqrt{N_0}$. We then keep all the remaining terms up to second order in the operators $b_{\mathbf{k}}$, with $\mathbf{k}\neq 0$, which includes anomalous terms corresponding to pair creation and annihilation from the condensate, and diagonalize this expression via a Bogoliubov transformation. The resulting dispersion relation is given by

$$\omega_{\mathbf{k}} = \sqrt{(\epsilon_{b,\mathbf{k}}-\epsilon_{b,0})(\epsilon_{b,\mathbf{k}}-\epsilon_{b,0}+2U_{bb}n_b)}, \quad (2)$$

where the bare lattice dispersion is given by:

$$\epsilon_{b,k} = -t_{b,1}2\cos k_x - t_{b,2}(2\cos(k_x/2+\sqrt{3}k_y/2) +2\cos(k_x/2-\sqrt{3}k_y/2)). \quad (3)$$

For small values of k_x and k_y, $\omega_{\mathbf{k}}$ can be expanded as:

$$\omega_{\mathbf{k}} \sim \sqrt{((2t_{b,1}+t_{b,2})k_x^2+3t_{b,2}k_y^2)U_{bb}n_b}, \quad (4)$$

which gives us the two velocities

$$v_{b,x} = \sqrt{(2t_{b,1}+t_{b,2})U_{bb}n_b} \quad (5)$$

$$v_{b,y} = \sqrt{3t_{b,2}U_{bb}n_b}. \quad (6)$$

In addition to the assumption that the bosons form a BEC, we assume that these velocities of the condensate fluctuations are much larger than the Fermi velocity, which corresponds to the conditions $v_{b,x/y}>t_{f,1/2}$.

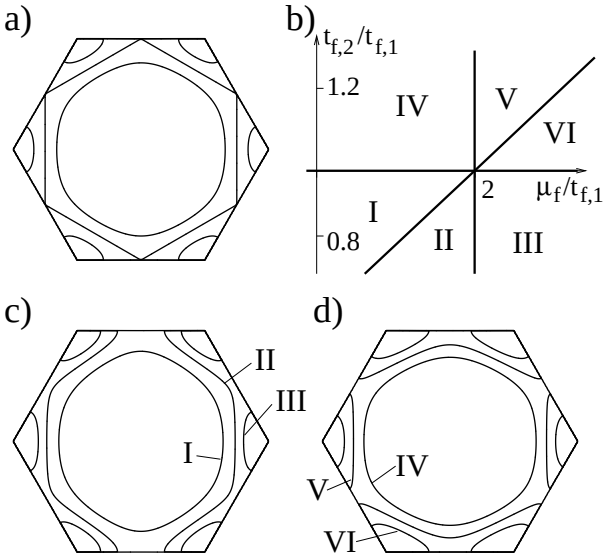

FIG. 1: a) Fermi surfaces for an isotropic lattice, for $\mu_f<2t_{f,1/2}$, $\mu_f=2t_{f,1/2}$ (hexagonal shape), and $\mu_f>2t_{f,1/2}$ (six disjoint arcs). b) Diagram of the different types of Fermi surfaces that can be created on an anisotropic lattice, by varying the ratio $t_{f,2}/t_{f,1}$ and μ_f. c) Fermi surfaces for $t_{f,2}<t_{f,1}$, for $\mu_f<4t_{f,2}-2t_{f,1}$, $4t_{f,2}-2t_{f,1}<\mu_f<2t_{f,1}$, and $\mu_f>2t_{f,1}$, corresponding to the regimes I–III, respectively. d) Fermi surfaces for $t_{f,2}>t_{f,1}$, for $\mu_f<2t_{f,1}$, $2t_{f,1}<\mu_f<4t_{f,2}-2t_{f,1}$, and $\mu_f>4t_{f,2}-2t_{f,1}$, corresponding to the regimes IV–VI, respectively.

Therefore, large bosonic hopping amplitudes, a bosonic density of $\approx$ 1–3, and some intermediate value for $t_{f,1/2}$ will satisfy this requirement. In this limit the bosonic modes can be integrated out, and one obtains an approximately non-retarded fermion-fermion interaction. The induced potential $V_{\mathrm{ind.},\mathbf{k}}$ is given by:

$$V_{\mathrm{ind.},\mathbf{k}} = -\tilde{V}/(1+\xi_1^2(2-2\cos k_x) +\xi_2^2(4-4\cos(k_x/2)\cos(\sqrt{3}k_y/2))), \quad (7)$$

with $\tilde{V}=U_{bf}^2/U_{bb}$, and ξ_a are the healing lengths of the Bose-Einstein condensate (BEC) and are given by $\xi_a=\sqrt{t_{b,a}/2n_bU_{bb}}$ with $a=1,2$. In summary, we arrive at a purely fermionic, non-retarded description of the form:

$$H_{\mathrm{eff.}} = \sum_{\mathbf{k}}\Bigg\{(\epsilon_{\mathbf{k}}-\mu_f)\sum_s f^\dagger_{\mathbf{k},s}f_{\mathbf{k},s}+\frac{U_{ff}}{V}\rho_{f,\mathbf{k},\uparrow}\rho_{f,-\mathbf{k},\downarrow} + \frac{1}{2V}V_{\mathrm{ind.},\mathbf{k}}\,\rho_{f,\mathbf{k}}\rho_{f,-\mathbf{k}}\Bigg\}, \quad (8)$$

This is the effective Hamiltonian that we study with a numerical implementation of the functional renormalization group.

III. FUNCTIONAL RENORMALIZATION GROUP

In this section we describe the numerical implementation of functional RG[23,24] that we use to study the effective Hamiltonian (8). In this approach we integrate the one-loop RG equations for the four-point interaction vertex $U(\mathbf{k}_1, \mathbf{k}_2, \mathbf{k}_3)$, which are functions of the direction of the momenta on the FS, with the fourth momentum not explicitly written, given by $\mathbf{k}_4 = \mathbf{k}_1 + \mathbf{k}_2 - \mathbf{k}_3$. We solve the RG equations for all the $U(\mathbf{k}_1, \mathbf{k}_2, \mathbf{k}_3)$[25], given by:

$$\begin{aligned}
&\partial_\ell U_\ell(\mathbf{k_1}, \mathbf{k_2}, \mathbf{k_3}) = \\
&-\int_{\mathbf{p},\omega} \Big\{ \partial_\ell [G_\ell(\mathbf{p},\omega) G_\ell(\mathbf{q_1},\omega)] U_{\tilde{\ell}'_{ph}}(\mathbf{p},\mathbf{k_1},\mathbf{k_4}) U_{\tilde{\ell}'_{ph}}(\mathbf{p},\mathbf{k_3},\mathbf{k_2}) \\
&+\partial_\ell [G_\ell(\mathbf{p},\omega) G_\ell(\mathbf{k},-\omega)] U_{\tilde{\ell}_{pp}}(\mathbf{k_1},\mathbf{k_2},\mathbf{p}) U_{\tilde{\ell}_{pp}}(\mathbf{k_3},\mathbf{k_4},\mathbf{p}) \\
&+\partial_\ell [G_\ell(\mathbf{p},\omega) G_\ell(\mathbf{q_2},\omega)] \Big\{ -2 U_{\tilde{\ell}_{ph}}(\mathbf{k_1},\mathbf{p},\mathbf{k_3}) U_{\tilde{\ell}_{ph}}(\mathbf{k_4},\mathbf{p},\mathbf{k_2}) \\
&+U_{\tilde{\ell}_{ph}}(\mathbf{p},\mathbf{k_1},\mathbf{k_3}) U_{\tilde{\ell}_{ph}}(\mathbf{k_4},\mathbf{p},\mathbf{k_2}) + U_{\tilde{\ell}_{ph}}(\mathbf{k_1},\mathbf{p},\mathbf{k_3}) U_{\tilde{\ell}_{ph}}(\mathbf{p},\mathbf{k_4},\mathbf{k_2}) \Big\} \Big\},
\end{aligned} \tag{9}$$

where $\ell = \ln(\Lambda_0/\Lambda)$ ($\Lambda_0 \approx 6t_f$ is a high-energy cut-off), $\mathbf{k} = \mathbf{k}_1 + \mathbf{k}_2 - \mathbf{p}$, $\mathbf{q_1} = \mathbf{p} + \mathbf{k}_1 - \mathbf{k}_4$, $\mathbf{q_2} = \mathbf{p} + \mathbf{k}_1 - \mathbf{k}_3$, $\tilde{\ell}_{pp} \equiv \min\{\ell_p, \ell_k\}$, $\tilde{\ell}'_{ph} \equiv \min\{\ell_p, \ell_{q_1}\}$,$\tilde{\ell}_{ph} \equiv \min\{\ell_p, \ell_{q_2}\}$, $\ell_p = \ln(\Lambda_0/|\xi_{\mathbf{p}}|)$, and $G_\ell(\mathbf{k},\omega) = \Theta(|\xi_{\mathbf{k}}| - \Lambda)/(i\omega - \xi_{\mathbf{k}})$ with $\xi_{\mathbf{k}} = \epsilon_{f,\mathbf{k}} - \mu_f$. The initial, i.e., bare value, of $U(\mathbf{k}_1, \mathbf{k}_2, \mathbf{k}_3)$ is given by:

$$U(\mathbf{k}_1, \mathbf{k}_2, \mathbf{k}_3) \;=\; U_{ff} + V_{\text{ind.},\mathbf{k}_1 - \mathbf{k}_3}\,. \tag{10}$$

From the vertex $U(\mathbf{k}_1, \mathbf{k}_2, \mathbf{k}_3)$ we obtain the possible many-body instability channels such as CDW$_i$, spin density wave (AF$_i$), where the index i refers to the three nesting vectors, and the superconducting (BCS) channel. These channels are given by:

$$V^{CDW_i} \;=\; 4\; U_c(\mathbf{k}_1, \mathbf{k}_2, \mathbf{k}_1 + \mathbf{Q}_i)\,, \tag{11}$$

$$V^{AF_i} \;=\; 4\; U_\sigma(\mathbf{k}_1, \mathbf{k}_2, \mathbf{k}_1 + \mathbf{Q}_i)\,, \tag{12}$$

$$V^{BCS} \;=\; U(\mathbf{k}_1, -\mathbf{k}_1, \mathbf{k}_2)\,, \tag{13}$$

For the isotropic case, perfect nesting occurs at 3/4-filling, with three possible nesting vectors: $\mathbf{Q}_1 = (0, 2\pi)$, $\mathbf{Q}_2 = (\pi, \sqrt{3}\pi)$, and $\mathbf{Q}_3 = (-\pi, \sqrt{3}\pi)$, leading to three different possible types of instabilities per density wave channel. For the anisotropic case, only $\mathbf{Q}_1$ can be a nesting vector, for the condition $\mu_f = 2t_{f,1}$.

To determine the scale of the gaps, Δ, associated with each of these order parameters, we use a 'poor man's' scaling estimate, specifically: $\Delta \approx \Lambda_0 e^{-\ell_c}$, where ℓ_c is the point at which the RG flow diverges and the instability occurs.

The RG is implemented numerically by discretizing the FS into $M = 24$ or 36 patches. The CDW and AF channel is represented by an $(M/3) \times (M/3)$ matrix, the BCS channel is represented by an $M \times M$ matrix, which are diagonalized at each RG step. The dominant instability is the channel that has an eigenvalue (divided by the dimension of the matrix) with the largest magnitude (for BCS one has to ensure that such eigenvalue is negative so that the channel is attractive). Each element of the corresponding eigenvector represents a given FS patch, and hence, the symmetry of the dominant order parameter is reflected on the patch (i.e., angular) dependence of each element around the FS. Using this method, we determine the phase diagram of the system in various limits.

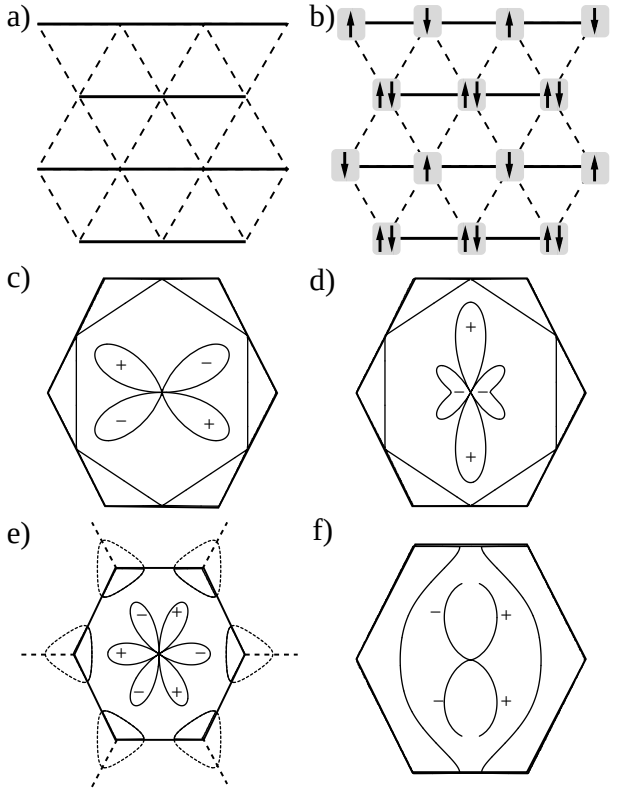

FIG. 2: a) Lattice geometry of the system. The continuous (dashed) bonds correspond to the hopping amplitudes $t_{b/f,1(2)}$. For $t_{b/f,1} = t_{b/f,2}$, the lattice is an isotropic triangular lattice. b) schematic representation of the AF order corresponding to nesting vector $\mathbf{Q}_1$. c) + d) Order parameters of the extended d-wave orders D_1 and D_2. e) Order parameter of the f-wave phase. This order can also be interpreted as two s-wave paired hole states whose order parameters are out of phase by π. f) Order parameter of the extended p-wave phase, that appears in anisotropic lattices.

IV. ISOTROPIC LATTICE

We first consider spin-1/2 fermions on an isotropic triangular lattice, i.e. with $t_{f,1} = t_{f,2} \equiv t_f$. The FS for such a lattice behaves as follows: For small filling the FS consists of one near-circular piece, which then approaches the shape of a hexagon as μ_f approaches the special value $\mu_f = 2t_f$. At this special chemical potential, which corresponds to 3/4-filling, the FS is nested

with the three distinct nesting vectors $\mathbf{Q}_i$. For filling fractions larger than 3/4 the FS breaks into six disjoined arcs. Examples for these different regimes are shown in Fig. 1 a). Without coupling to the BEC, the fermions form an s-wave pairing phase for attractive interactions, and a Fermi liquid phase for repulsive interactions[26], except for the specific case $\mu_f = 2t_f$, where the system shows AF order for repulsive interactions. A schematic picture of this order is shown in Fig. 2 b) for the nesting vector $\mathbf{Q}_1$.

We found a similar behavior for an isotropic square lattice in [16], s-wave pairing for attractive interaction, and Fermi liquid behavior for repulsive interaction, except at half-filling, for which we find AF order. An interesting difference for the triangular lattice is the three-fold degeneracy of the AF phase, an indication of frustration.

When one turns on the coupling to the BEC, the isotropic system shows a phase diagram of the type shown in Fig. 3. The s-wave pairing phase slightly extends into the regime of positive U_{ff}, because of the induced attractive interaction mediated by the bosonic fluctuations. The regime that showed Fermi liquid behavior in the absence of the induced interaction now shows a rich competition of various types of pairing. In the regime where the density is below half-filling, when the FS is approximately circular, the system shows p-wave pairing. For fillings larger than 3/4, when the FS consists of six disjoined parts, the fermions Cooper pair in a superconducting state with f symmetry. As shown in Fig. 2 e), the FS in this regime can also be interpreted as two distinct near-circular FSs of holes. In this interpretation each of these two fermionic systems is in an s-wave pairing phase, but the relative phase between the two order parameters is π. At 3/4-filling and large values of U_{ff}, the system still shows AF order. However, for smaller values of U_{ff}, and also for smaller fillings, two phases with degenerate extended d symmetry develop. These superconducting orders have a sizeable g-wave component and are approximately given by:

$$\psi_{D_1} = \sin 2\theta + 0.5 \sin 4\theta \quad (14)$$

$$\psi_{D_2} = \cos 2\theta - 0.5 \cos 4\theta \quad (15)$$

These order parameters are shown in Fig. 2 c) and d). The shapes of the order parameters are energetically advantageous because, on the one hand, the order parameter maxima are located at points at which the system has a high density of states (the 'corners' of the FS). Hence, when the superconducting gap opens, there is a large gain of condensation energy coming from these regions on the FS. On the other hand, the d-wave state has lower kinetic energy than the f-wave, and hence is selected.

The phase diagram Fig. 3 has a number of similarities to the phase diagram for a BFM on a square lattice, such as the s- and the p-wave pairing phase, and the existence of AF order for a nested Fermi surface for large U_{ff}. However, the competition of pairing orders for positive U_{ff} and intermediate and large filling is much richer, due to the more complex shape of the Fermi surface.

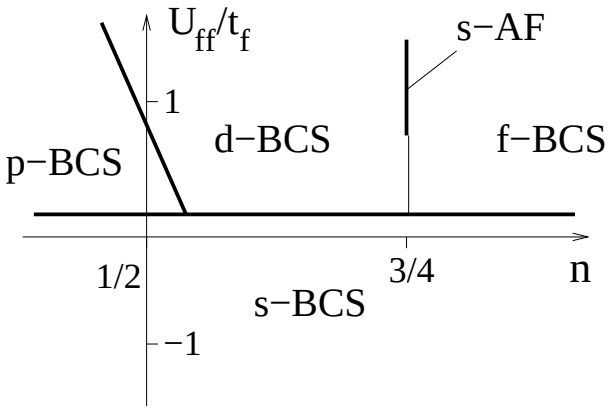

FIG. 3: Phase diagram of a Bose-Fermi mixture on a 2D isotropic triangular lattice. The vertical axis corresponds to the interaction strength, U_{ff}/t_f, whereas the horizontal axis corresponds to the filling fraction of the fermions per site, n. The other parameters are given by $\tilde{V}/t_f = 3$, and $\xi_a = 1$ with $a = 1, 2$.

The energy gaps associated with these order parameters can be determined as we did in [16], by using a 'poor man's' scaling argument. We find for the s-wave pairing and the AF order, that they are around $0.1T_F$, where T_F is the Fermi temperature of the system. For most of the exotic phases, we energy gaps of the order of $0.01 - 0.001T_F$.

V. ANISOTROPIC LATTICE

We now consider a BFM with spin-1/2 fermions on an anisotropic triangular lattice, i.e. with unequal hopping amplitudes, $t_{f(b),1} \neq t_{f(b),2}$. The shape of the FS behaves as follows: For $t_{f,2} > t_{f,1}$, as one increases the chemical potential, the FS first breaks into four arcs at $\mu_f = 2t_{f,1}$, and then breaks into six arcs at $\mu_f = 4t_{f,2} - 2t_{f,1}$, corresponding to the regimes IV–VI, in Fig. 1 b) and d). For $t_{f,2} < t_{f,1}$ the FS first breaks into two arcs at $\mu_f = 4t_{f,2} - 2t_{f,1}$, and then breaks into six arcs at $\mu_f = 2t_{f,1}$ coresponding to the regimes I–III, in Fig. 1 b) and c). At the special chemical potential $\mu_f = 2t_{f,1}$ the FS is still nested, but there is only one nesting vector along the direction of the bonds with hopping amplitude $t_{f,1}$. In the absence of the coupling to the BEC the phase diagram has a similar structure as for the isotropic case: s-wave pairing for attractive interaction, Fermi liquid behavior for repulsive interaction, with the exception of the nested FS at $\mu_f = 2t_{f,1}$ where one finds AF order (notice that in this case the filling is not 3/4).

When the coupling to the bosons is turned on, one generates an even more complicated competition of pairing phases for repulsive U_{ff} in the vicinity of the point $\mu_f = 2t_{f,1}$, as is shown in Fig. 4. Generally, for unequal hopping the degeneracy between D_1 and D_2 in (15), as well as p_x and p_y is lifted: In the regime with

$t_{f,2} > t_{f,1}$ ($t_{f,2} < t_{f,1}$), D_1 (D_2) and p_x (p_y) dominate. For $t_{f,2} > t_{f,1}$, in the intermediate regime, in which the FS consists of four disjoined arcs, corresponding to the regime V in Fig. 1, the type of ordering changes from D_1 to f. For $t_{f,2} < t_{f,1}$, the type of pairing also eventually becomes f-wave, but first develops two other types of pairing, in the regime II in Fig. 1. Firstly, one finds an unusual extended p-wave symmetry, which is schematically shown in Fig. 2 f). Its wavefunction is of the form:

$$\psi_{P_{ext}} = \begin{cases} \sin^2\theta & -\pi/2 < \theta < \pi/2 \\ -\sin^2\theta & \pi/2 < \theta < 3\pi/2 \end{cases} \qquad (16)$$

The second type of pairing that appears before the system develops f-wave pairing is D_1. These unusual pairing states are energetically favorable because of the anisotropic shape of the FS. For the regime in which the FS has just barely broken up into two arcs, the order parameter assumes p-wave symmetry and the maxima are located along the y-axis, where the density of states is highest. As the region of open FS widens (see Fig. 2 f)), this pairing becomes energetically unfavorable, and the system develops D_1-pairing, so that the maxima of the order parameter can again be located near the point of highest density of states. The energy gaps associated with these order parameters are of the same order of magnitude as for the isotropic lattice.

VI. SPINLESS FERMIONS

Finally, we consider a BFM with spinless fermions on an isotropic lattice. Due to the absence of s-wave scattering between fermions of the same spin state, there is no direct interaction, that is, $U_{ff} = 0$. Hence, in the absence of bosons, the spinless gas is non-interacting. The boson fluctuations, however, mediate an induced interaction between the fermions. Due to the anti-symmetry of the Cooper pair wavefunction, pairing occurs in an odd angular momentum channel. We find a competition between p and f-wave pairing symmetry. For small to intermediate filling ($n < 0.65$), p-wave pairing dominates. For larger fillings, for which the FS first approaches the shape of a hexagon and then breaks up into six arcs, the system shows f-wave pairing. Since these larger fillings of fermions are typically realized in the center of an atomic trap, this result would suggest a comparatively easy way to create an exotic pairing state experimentally.

In contrast to this, a spinless BFM on a square lattice only shows p-wave pairing, since for the quadrangular shape of its FS, channels of higher angular momentum are of no advantage energetically.

VII. CONCLUSION

We have used a functional RG approach to study BFM of ultra-cold atoms, both with spin-1/2 and with spinless fermions, in a 2D optical lattice with triangular geometry. We found a number of competing types of order: For an isotropic lattice, we found pairing states with s, p-, extended d-, and f-wave symmetry, as well as AF order. For an anisotropic lattice, we additionally found extended p-wave pairing, and that the degeneracy between the two types of extended d-wave pairing and the two types of p-wave pairing has been lifted. For a BFM with spinless fermions, we found a competition between p- and f-wave pairing. From the RG flow we also identified the magnitude of the superconducting gaps, which turn out to be a fraction of the Fermi temperature, of the order of $0.01T_F$–$0.001T_F$. Nevertheless, it is possible to increase these gaps substantially if the coupling to the BEC is in the strong-coupling regime. In this case, retardation effects can enhance the pairing mechanisms substantially requiring an Eliashberg theory instead of BCS. To take into account retardation effects in this problem, the frequency dependence of U should also be kept[29]. The functional RG method with frequency dependence can be used in this regime.

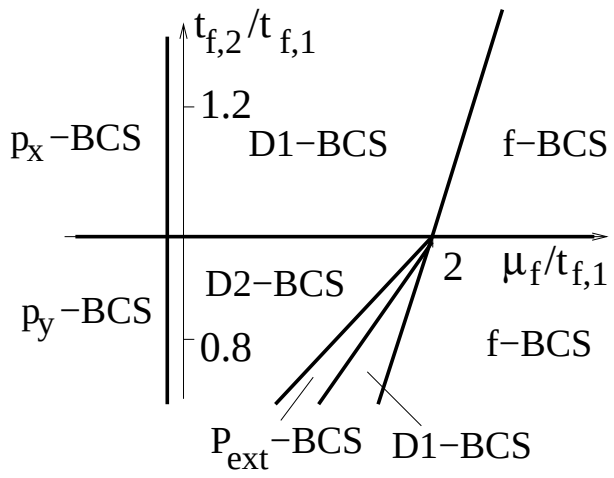

FIG. 4: Phase diagram of a Bose-Fermi mixture on an anisotropic triangular lattice. The vertical axis corresponds to the ratio $t_{f,2}/t_{f,1}$, the horizontal axis corresponds to the chemical potential μ_f. The other parameters are given by $\tilde{V}/t_f = 3$, $U_{ff}/t_{f,1} = 2$, and $\xi_a = 1$ with $a = 1, 2$).

An important question in the context of ultracold atoms concerns the detectability of these phases. The exotic superconducting and AF states discussed in this work exhibit distinct experimental signatures. The AF state can be studied via time-of-flight images and Bragg scattering[27], and the different superconducting phases can be measured through noise correlations[8]. Finally, laser stirring experiments[28] can be used to establish the phase boundary between two phases.

In conclusion, we presented a systematic study of the weak-coupling limit of BFMs of ultracold atoms in triangular optical lattices. For the various regimes, we found a number of exotic phases, and discussed their properties and their relevance for ultra-cold atom experiments.

Given the generic structure of the Hamiltonian that we considered, the new types of phases, such as the extended d-wave pairing phase and the extended p-wave phases, are also of interest for the study of solid-state systems with triangular symmetry.

We thank A. Polkovnikov for illuminating conversations. A. H. C. N. was supported by the NSF grant DMR-0343790.

[1] T. Stöferle, H. Moritz, C. Schori, M. Köhl, and T. Esslinger, Phys. Rev. Lett. **92**, 130403 (2004).

[2] O. Mandel, M. Greiner, A. Widera, T. Rom, T. W. Hänsch, and I. Bloch, Phys. Rev. Lett. **91**, 010407 (2003); O. Mandel, M. Greiner, A. Widera, T. Rom, T. W. Hänsch, and I. Bloch, Nature (London) **425**, 937 (2003).

[3] M. Köhl, H. Moritz, T. Stöferle, K. Günter, and T. Esslinger, Phys. Rev. Lett. **94**, 080403 (2005).

[4] M. Greiner, O. Mandel, T. Esslinger, T. W. Hänsch, and I. Bloch, Nature (London) **415**, 39 (2002).

[5] M. Greiner, C. A. Regal, and D. S. Jin, Nature **426**, 537 (2003); S. Jochim, M. Bartenstein, A. Altmeyer, G. Hendl, S. Riedl, C. Chin, J. Hecker Denschlag, and R. Grimm, Science **302**, 2101 (2003); M.W. Zwierlein, C.A. Stan, C.H. Schunck, S.M.F. Raupach, S. Gupta, Z. Hadzibabic, and W. Ketterle, Phys. Rev. Lett. **91**, 250401 (2003).

[6] B. Paredes, A. Widera, V. Murg, O. Mandel, S. Foelling, I. Cirac, G. V. Shlyapnikov, T. W. Hänsch, and I. Bloch, Nature **429**, 277 (2004).

[7] H. Moritz, T. Stöferle, K. Günter, M. Köhl, and T. Esslinger, Phys. Rev. Lett. **94**, 210401 (2005).

[8] M. Greiner, C. A. Regal, J. T. Stewart, and D. S. Jin, Phys. Rev. Lett. **94**, 110401 (2005); S. Foelling, F. Gerbier, A. Widera, O. Mandel, T. Gericke, and I. Bloch, Nature **434**, 481 (2005); E. Altman, E. Demler, and M. D. Lukin, Phys. Rev. A **70**, 013603 (2004); L. Mathey, E. Altman, and A.Vishwanath, cond-mat/0507108.

[9] G. Modugno, G. Roati, F. Riboli, F. Ferlaino, R. J. Brecha, and M. Inguscio, Science, **297**, 2240 (2002); J. Goldwin, S. Inouye, M. L. Olsen, B. Newman, B. D. DePaola, and D. S. Jin, Phys. Rev. A **70**, 021601 (2004).

[10] S. Ospelkaus, C. Ospelkaus, O. Wille, M. Succo, P. Ernst, K. Sengstock, and K. Bongs, Phys. Rev. Lett. **96**, 180403 (2006); K. Günter, T. Stöferle, H. Moritz, M. Köhl, and T. Esslinger, Phys. Rev. Lett. **96**, 180402 (2006).

[11] R. Roth and K. Burnett, Phys. Rev. A **69**, 021601 (2004); T. Miyakawa, H. Yabu, and T. Suzuki, cond-mat/0401107; H.P. Büchler and G. Blatter, Phys. Rev. Lett. **91**, 130404 (2004); cond-mat/0402432.

[13] M.Y. Kagan, H. Yabu, and T. Suzuki, cond-mat/0401107; H.P. Büchler and G. Blatter, Phys. Rev. Lett. **91**, 130404 (2004); cond-mat/0402432.

[13] M.Y. Kagan, I.V. Brodsky, D.V. Efremov, and A.V. Klaptsov, cond-mat/0209481; M. Lewenstein, L. Santos, M. A. Baranov, and H. Fehrmann, Phys. Rev. Lett. **92**, 050401 (2004); H. Fehrmann, M. A. Baranov, B. Damski, M. Lewenstein, and L. Santos, cond-mat/0307635; A. Albus, F. Illuminati, and J. Eisert, Phys. Rev. A 68, 023606 (2003).

[14] L. Mathey, D.-W. Wang, W. Hofstetter, M. D. Lukin, and E. Demler, Phys. Rev. Lett. **93**, 120404 (2004); L. Mathey, and D.-W. Wang, Phys. Rev. A 75, 013612 (2007).

[15] R. B. Diener, and T.-L.Ho, Phys. Rev. Lett. **96**, 010402 (2006).

[16] L. Mathey, S.-W. Tsai, and A. H. Castro Neto, Phys. Rev. Lett. **97**, 030601 (2006).

[17] K. Takada, H. Sakurai, E. Takayama-Muromachi, F. Izumi, R. A. Dilanian, and T. Sasaki, Nature **422**, 53 (2003).

[18] R. L. Withers and J. A. Wilson, J. Phys. C **19**, 4809 (1986).

[19] D. Jerome, Science **252**, 1509 (1991).

[20] H. Kino and H. Fukuyama, J. Phys. Soc. Jpn. **64**, 2726 (1995); R. H. Mckenzie, Science **278**, 820 (1997).

[21] S.-W. Tsai and J. B. Marston, Can. J. Phys. **79** 1463 (2001); C. Honerkamp, Phys. Rev. B **68**, 104510 (2003).

[22] M. Vojta and E. Dagotto, Phys. Rev. B **59**, 713 (1999); G. Baskaran, Phys. Rev. Lett. **91**, 097003 (2003); S.-S. Lee and P. A. Lee, Phys. Rev. Lett. **95**, 036403 (2005); T.-P. Choy, D. Galanakis, and P. Phillips, cond-mat/0502164; J. Y. Gan, Y. Chen, and F. C. Zhang, Phys. Rev. B **74**, 094515 (2006); A. Zhou and Z. Wang, cond-mat/0608068.

[23] R. Shankar, Rev. Mod. Phys. **66**, 129 (1994).

[24] D. Zanchi and H.J. Schulz, Phys. Rev B **61**, 13609 (2000).

[25] $U(\mathbf{k}_1, \mathbf{k}_2, \mathbf{k}_3)$ denotes processes involving electrons with opposite spins. Processes involving parallel spins can be obtained from these[24].

[26] We ignore high angular momentum pairing phases predicted by the Kohn-Luttinger theorem which would occur at energy scales much lower than the experimentally accessible regime.

[27] J.Stenger, S. Inouye, A.P. Chikkatur, D.M. Stamper–Kurn, D.E. Pritchard, and W. Ketterle, Phys. Rev. Lett. **82**, 4569 (1999).

[28] C. Raman, M. Köhl, R. Onofrio, D. S. Durfee, C. E. Kuklewicz, Z. Hadzibabic, and W. Ketterle, Phys. Rev. Lett. **83**, 2502 (1999); R. Onofrio, C. Raman, J. M. Vogels, J. R. Abo-Shaeer, A. P. Chikkatur, and W. Ketterle, Phys. Rev. Lett. **85**, 2228 (1999).

[29] S.-W. Tsai, A.H. Castro Neto, R. Shankar, and D.K. Campbell, Phys. Rev. B **72**, 054531 (2005); *ibid.*, Philos. Mag., **86**, 2631 (2006).